Molecular Dynamics Simulations of LiCo$_y$Mn$_{2−y}$O$_4$ Cathode Materials for Rechargeable Li Ion Batteries

Masanobu Nakayama,[†] Mayumi Kaneko,[†] Yoshiharu Uchimoto,[†] Masataka Wakihara,*,[†] and Katsuyuki Kawamura[‡]

Department of Applied Chemistry, Tokyo Institute of Technology, Ookayama, Meguro-ku, Tokyo 152-8552, Japan, and Department of Earth and Planet Science, Tokyo Institute of Technology, Ookayama, Meguro-ku, Tokyo 152-8552, Japan

Received: November 10, 2003; In Final Form: January 26, 2004

Molecular dynamics (MD) simulations have been performed for the spinel solid−solution, LiCo$_y$Mn$_{2−y}$O$_4$ in combination with experimental methods, X-ray diffraction (XRD), and infrared spectroscopy. The partial ionic potential model was used and optimized in the present MD simulation study. It showed good accordance with the observed lattice parameter on various Co contents and temperature. From the analysis of simulated results, it was concluded that the local distortion was caused by the mismatch of ionic size between Mn^{3+} and Mn^{4+} via the 16c vacancy site, and the Co substitution suppressed the local distortion in the lattice. The dynamical properties based on the simulated results were also analyzed and compared with experimental infrared absorption spectra. The reinforcement of chemical bonds by Co substitution was indicated in the simulation results, and it was supported by infrared absorption spectra.

Introduction

Development of LiMn$_2$O$_4$ spinel oxides as the cathode material for lithium ion batteries is vital due to its low cost, low toxicity, relatively high energy density, and so forth.[1−3] However, this material shows marked capacity fade during charge−discharge cycles. To improve the cycle performance, several research groups have investigated the electrochemical properties of partially metal-substituted spinels LiM$_y$Mn$_{2−y}$O$_4$ (M = Al, Cr, Ga, Ti, Ge, Fe, Co, Zn, Ni, Mg),[4−10] and significant improvement of cyclability was shown for substitution, such as Co^{3+}, Cr^{3+}, and Ni^{2+}. Although the mechanism for their improvement was proposed by several researchers, such as decreasing the Mn ion dissolution into electrolyte solutions,[11] restraint of Jahn−Teller distortion arising from the Mn^{3+} ion,[2,3,12] and reinforcement of the chemical bond between transition metals and oxide ions,[2,6] the exact factor is still ambiguous. To elucidate the mechanism, the investigation of the crystal structure of LiMn$_2$O$_4$ and related materials was extensively studied by diffraction technique.[13−17] The spinel LiMn$_2$O$_4$ belongs to cubic space group *Fd3m* with eight AB$_2$X$_4$ units per unit cell in which lithium ions locate at the tetrahedral 8a sites, manganese ions (Mn^{3+} and Mn^{4+}) at the octahedral 16d sites, and oxide ions at the 32e sites. However, the diffraction techniques only give the averaged arrangement of ions, or lack information on the local environmental structure. Generally, the substitution induces local structural modifications in the lattice, which would affect the stability of the crystal and lithium diffusion property, etc. and affect the electrochemical performance of the cathode material. Therefore, investigation of the local environmental structure is important to understand electrochemical properties. In this viewpoint, there are some reports on the local structure around the transition metal ion in

the LiMn$_2$O$_4$ and related materials using X-ray absorption fine structure (XAFS) measurement[18−24] and molecular dynamics (MD) simulation.[24−31] Especially, MD simulation is well suited to explore solid-state materials at the atomic level and has been applied successfully to various systems, including studies of the lithium insertion/extraction reaction at Fe$_3$O$_4$[32] and Li$_x$Mn$_2$O$_4$ related materials.[24−31] Among them, Islam et al.[25−28,30] reported that the local structural perturbation due to its vacancies, substitutions and proton insertion affected the stability of the systems, the migration of the lithium ions, and lithium ordering effects of the materials. Recently, we have reported the detailed local structure of the Cr doped spinels by molecular dynamics (MD) simulation in combination with XAFS technique.[24] The study has revealed that the local distortion is caused by the size difference between Mn^{3+} and Mn^{4+} ions and is suppressed by Cr substitution. Furthermore, it has also reinforced the metal-oxide ion bond strength with Cr substitution by interpretation of simulated potentials, and we have suggested the positive relationship between cyclability and bond strength.

In the present paper, to clarify the suggested relationships, the Co doped spinels, LiCo$_y$Mn$_{2−y}$O$_4$, were synthesized and investigated by the MD simulation in view of local distortion and dynamic property of the lattice. Especially, the dynamic property is directly related to the vibrational spectra. For example, Julien et al. reported systematically the vibrational spectra on LiMn$_2$O$_4$ spinels regarding the local environment model.[33] Therefore, the infrared absorption spectra also adopted and referred to the simulation results. In addition, the dynamic properties of Cr doped spinels were also investigated using the MD technique with previously optimized potential parameters[24] to compare with the Co doped one.

Methods

Experimental Section. The stoichiometric compounds LiCo$_y$Mn$_{2−y}$O$_4$ ($0 \leq y \leq 1.0$) were synthesized by solid-state reaction. The reagents Li$_2$CO$_3$, Co(COO)$_2$·2H$_2$O, and Mn$_2$O$_3$

* Corresponding author. Tel.: + 81 3 5734 2145. Fax: +81 3 5734 2146.
† Department of Applied Chemistry.
‡ Department of Earth and Planet Science.

were used as starting materials. The mixtures were heated at 820 °C for 3 days in air, and cooled with a rate of 0.5 °C/min.

The chemical composition of each sample was evaluated by ICP measurement after dissolving the oxide in diluted sulfuric acid using SPS-1500VR (Prodigy Leeman Labs/JEOL Datum). The obtained composition is Li$_{1.02}$Mn$_2$O$_4$ and Li$_{0.98}$Co$_{1.02}$Mn$_{0.98}$O$_4$, and they were consistent with the ideal ones, LiMn$_2$O$_4$ and LiCoMnO$_4$, respectively, within experimental error (hereinafter, the samples were indicated with the formula LiCo$_y$Mn$_{2-y}$O$_4$).

The phase identification and the evaluation of lattice parameters were carried out by powder X-ray diffraction using Cu Kα radiation (RINT-2500V, Rigaku Co. Ltd). Through the XRD pattern analysis, the lattice parameter refinement was performed in each temperature from 25 to 300 °C. The lattice parameters were determined by the 2θ values of observed peak top (60° ≤ 2θ ≤ 120°) using the software of least-squares method resident on the RINT-2500V diffractmeter, and silicon powder was used as an internal standard.

The infrared absorption data were recorded at room temperature using a JASCO FT/IR-350 spectrometer with the sample disk dispersed in the KBr powder. The spectra of Cr doped samples, LiCr$_y$Mn$_{2-y}$O$_4$ (0 ≤ y ≤ 1.0), were also measured. (The synthesis procedure and results of phase characterization of Cr doped samples were already mentioned in a previous report.[24])

MD Simulation Procedure. The interatomic potential along with a partially ionic model, i.e., the two-body central force interatomic potential terms that depend only on the distance of ion pairs i and j, was adopted in the present study.

The interatomic potential is expressed by

$$U_{ij} = \frac{z_i z_j e^2}{r_{ij}} + f_0(b_i + b_j)\exp\left(\frac{a_i + a_j - r_{ij}}{b_i + b_j}\right) - \frac{c_i c_j}{r_{ij}^6} +$$
$$D_{ij}\{\exp[-2\beta_{ij}(r_{ij} - r_{ij}^*)] - 2\exp[-\beta_{ij}(r_{ij} - r_{ij}^*)]\} \quad (1)$$

The first term in eq 1 represents the Columbic interaction where z_i and z_j are the effective charges of the ions i and j, respectively, and r_{ij} is the interatomic distance between the ions. The second term represents the short-range repulsion potential. The parameters a_i and a_j relate to the ionic radii, and b_i and b_j correspond to the hardness of the ions. f_0 is a constant (6.9478 × 10^{-11} N). The third term represents the dipole induced dipole dispersion potential based on van der Waals interaction. The last term is the Morse potential to reproduce another type of interaction, such as the covalency effect. D_{ij}, β_{ij}, and r^* are the specific parameters of the bond between the i and j ions. Note that the covalent character of Li−O was excluded in this simulation due to the strong ionic character of the lithium ion. Katsumata et al.[34] pointed out that the partially ionic model described by eq 1 well reproduces the compressibility and thermal expansion coefficients observed in the perovskite-type La$_{0.6}$Li$_{0.2}$TiO$_3$, comparing with the fully ionic potential model using first three terms of eq 1. Because the compressibility and thermal expansion coefficients deeply depend on the shape of the potential well around atomic sites and are related to the bond strength mentioned in the Introduction, the partially ionic model was used in this study.

Each potential parameter of Li, Mn, O, and the Mn−O pair for MD simulation has been already described in our previous paper.[24] The parameters of the Co^{3+} ion and Co−O pair were
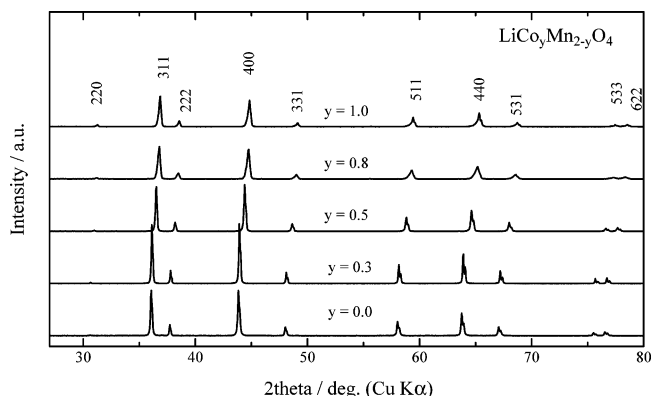

Figure 1. Powder XRD patterns of LiCo$_y$Mn$_{2-y}$O$_4$ (y = 0.0, 0.3, 0.5, 0.8, 1.0).

determined by trial and error. The detailed procedure has been already mentioned in ref 24. The simulation was performed using MXDORTO code developed by Kawamura.[35] The Verlet algorithm was used for the calculation of the atomic motions, and the Ewald method was applied to the calculations of the electrostatic interactions. The cell for the MD simulation was composed of 7000 particles (5 × 5 × 5 unit cells), and Mn^{3+}, Mn^{4+}, and Co^{3+} ions are distributed randomly in the 16d sites (the assumption was based on the previous results that the cation ordering observed in Ni^{36} or Mg^{37,38} doped spinels was not observed by XRD analysis,[38] neutron diffraction,[39] vibrational spectroscopic technique,[39] and the EXAFS analysis of Co doped spinel oxides[21]). Periodic boundary conditions were used with the MD basic cell. The calculations were performed using (N, P, T) ensemble at 298 K for 15 000 steps with a time step of 2 fs.

Relevant correlation functions were computed to study the dynamical properties for the end composition of spinels, LiMn$_2$O$_4$, LiCoMnO$_4$, and LiCrMnO$_4$ (in the case of Cr doped sample, the potential parameters optimized in the previous paper [24] were used for the simulation). For single particle dynamics, the power spectrum, which related to the vibrational density of states (DOS), is simply the Fourier transform of the atom velocity autocorrelation function,

$$\text{DOS} = \int_0^\infty \exp(-i\omega t)\langle v(t)\cdot v(0)\rangle \, dt \quad (2)$$

where

$$\langle v(t)\cdot v(0)\rangle = \sum_{i=1}^N \langle v_i(t)\cdot v_i(0)\rangle \quad (3)$$

The integration in eq 2 was calculated in a time step of 2 fs for a time duration of 200 ps (100 000 steps) after an initial equilibration period of 20 ps. The autocorrelation functions were sufficiently converged. The vibrational DOS of each ion in the spinel structure was calculated independently.

Results and Discussion

Structural Analysis by XRD. The XRD patterns and refined lattice parameters of LiCo$_y$Mn$_{2-y}$O$_4$ (0 ≤ y ≤ 1) are shown in Figures1 and 2, respectively. Under our experimental conditions, the only spinel phase was observed in the composition range y = 0 to 1. The cubic lattice parameter decreased monotonically with Co substitution. The obtained lattice parameters were used for the initial structural parameters of MD simulation.
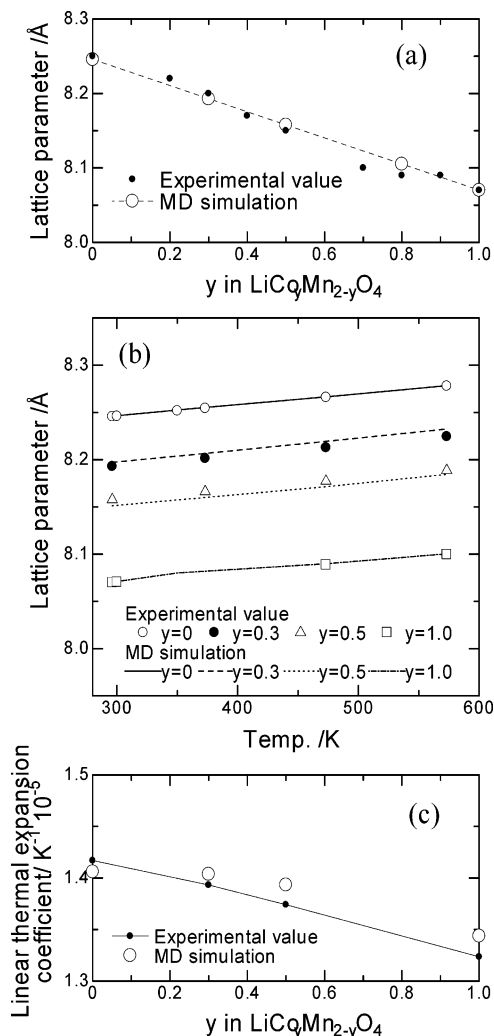
Figure 2. Comparison of the lattice parameter between experimental values and simulated values as a function of (a) y in $LiCo_yMn_{2-y}O_4$ and (b) temperature for $LiCo_yMn_{2-y}O_4$. The linear thermal expansion coefficient was also plotted on (c) as a function of the composition y.

Infrared Absorption Spectra. Figure 3 shows the infrared absorption spectra for Co doped and Cr doped samples. Two absorption peaks were observed in all samples and assigned as the T_{1u} mode for both peaks according to the literature.[26] As seen in the figure, both peaks of the spectra shifted to higher wavenumber side with Co and/or Cr substitution. In the simple form of the two-atom interaction model, the peak wavenumber is a function of the bond strength k and reduced mass μ. In the present case, it is concluded that Co and/or Cr substitution strengthens the chemical bond in the lattice, because the difference of reduced mass would be neglected due to their close value of atomic mass for Co (58.933), Cr (51.996), and Mn (52.938). However, the infrared spectra only show the specific vibration mode determined by the selection rule;[40] therefore, the analysis of total vibrational DOS is necessary for the estimation whether chemical bond is strengthen by the substitution or not.

Molecular Dynamics Simulation. The optimized potential parameters using the present study (including vibrational DOS calculation) are listed in Table 1. The validity of the optimized values for Co doped spinels were evaluated by the compositional dependence of lattice parameters and linear thermal expansion coefficients at room temperature. (Note that the validity of Cr substituted one is already confirmed in the previous paper.[24]) The linear thermal expansion coefficients β were obtained by
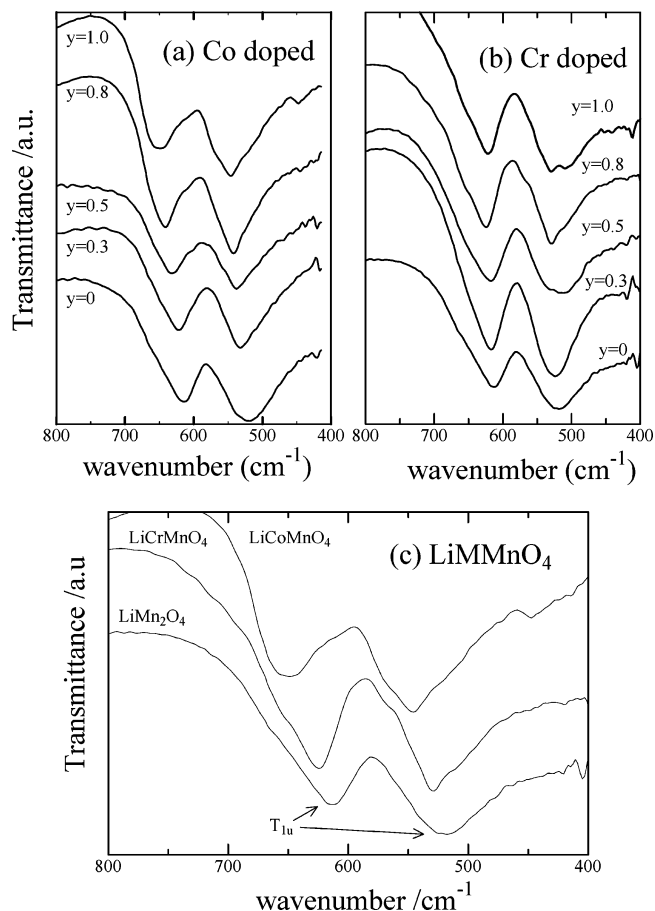

Figure 3. Infrared absorption spectra for (a) $LiCo_yMn_{2-y}O_4$ and (b) $LiCr_yMn_{2-y}O_4$. (c) The comparison of absorption peak among the end members of spinels, $LiMn_2O_4$, $LiCoMnO_4$, and $LiCrMnO_4$, respectively.

TABLE 1: Potential Parameter of Each Ion and Ion Pair for Eq 1

ion	z/e	$a/Å$	$b/Å$	$c/(kJ\ mol^{-1})^{1/2}\ Å^{-3}$
Li^a	1.0000	1.0010	0.08	1.64
$Mn^{4+\ a}$	2.2000	0.8189	0.10	0.00
$Mn^{3+\ a}$	1.6500	0.8519	0.10	0.00
$Cr^{3+\ a}$	1.6500	0.9328	0.10	0.00
Co^{3+}	1.6500	0.9328	0.10	0.00
$O^{2-\ a}$	−1.2125	1.9265	0.18	40.91

ion pair	$D/kJ\ mol^{-1}$	$\beta/Å^{-1}$	$r*/Å$
$Mn^{4+}-O^a$	12.21	2.00	2.00
$Mn^{3+}-O^a$	9.53	2.00	2.10
$Cr^{3+}-O^a$	15.39	2.00	1.99
$Co^{3+}-O^a$	16.31	2.00	1.94

^{a} Reference 22.

the following equation:

$$\beta = \frac{1}{L_{RT}}\left(\frac{\partial L(T)}{\partial T}\right)_p \qquad (4)$$

where T indicates the temperature (K), and L_{RT} and $L(T)$ indicate the lattice parameters at room temperature and temperature T (K), respectively. The simulated results of the lattice parameter with various compositions and temperatures are plotted in the Figure 2 and summarized in Table 2. A good accordance with experimental data is observed, or an appropriateness of potential parameter was confirmed in the case of Co substituted samples.

To investigate the microscopic structure, the pair correlation functions (pcf), $g_{ij}(r)$, of the $M_{16d}-O$ and $O-O$ interactions in

TABLE 2: Lattice Parameters and Linear Thermal Expansion Coefficients of LiCo$_y$Mn$_{2-y}$O$_4$

composition	lattice params (room temp)		linear thermal expansion coeff (room temp)	
y	a(exp)/Å	a(simul)/Å	$10^5\beta$(exp)/K^{-1}	$10^5\beta$(simul)/K^{-1}
0.0	8.24774(7)	8.24569(86)	1.417	1.406
0.3	8.19612(2)	8.19297(84)	1.393	1.404
0.5	8.14845(6)	8.15774(79)	1.374	1.393
0.8	8.0931(1)	8.10519(79)		
1.0	8.0730(1)	8.07027(77)	1.324	1.344

LiCo$_y$Mn$_{2-y}$O$_4$ were calculated using the following equation:

$$g_{ij}(r) = \frac{n_{ij}(r)}{4\pi(N_iN_j/V)r^2\Delta r} \tag{5}$$

where N_i and N_j are the number of ions in the basic cell with volume V, and $n_{ij}(r)$ is the number of the pair of ion i and ion j between the distance of $r - (\Delta r/2)$ and $r + (\Delta r/2)$, where Δr is 1 pm. The results of calculated pcf at 298K are shown in Figure 4 for the case of end members of composition. In Figure 4a, the peak top of each pcf curve relates to the bond length of M−O (M = Co, Mn). The bond length of M−O showed the following relationships; Mn^{3+}−O > Co^{3+}−O > Mn^{4+}−O, and the Mn^{4+}−O distances of both LiMn$_2$O$_4$ and LiCoMnO$_4$ were quite similar, whereas the Co^{3+}−O distance is shorter than Mn^{3+}−O. This behavior could be understood from the idea of ionic radius; i.e., the Co^{3+} ion ionic radius (0.545 Å[41]) is smaller than that of the Mn^{3+} ion (0.645 Å[41]) and is close to that of the Mn^{4+} ion (0.530 Å[41]). To evaluate the local distortion more quantitatively, the standard deviations σ (or peak broadness) of M−O were calculated and presented in Figure 5 as a function of composition y. As shown in the figure, all of the σ for M−O bonds decreased with the substitution of Co, indicating the local distortion decreases with composition y. A similar behavior also reported by Aitchison et al.[21] using the EXAFS technique, the Debye−Waller factors of the Mn−O interaction decreasing with composition x in the LiCo$_x$Mn$_{2-x}$O$_4$. (However, no clear correlation was observed in the case of Co−O interaction probably due to the experimental limitation of EXAFS analysis. In addition, the EXAFS analysis at room temperature cannot distinguish Mn^{4+} and Mn^{3+}. On the other hand, the pcf of the MD simulation clearly indicated the difference, as shown in the figure.) Therefore, the present results show the suppression of local distortion by the substitution of Co^{3+}. Note that, in the case of Cr substitution, the same conclusion has been already obtained in our previous study through the study of EXAFS and MD.[24]

To discuss the detailed mechanism of suppression of the local distortion, the O−O interaction was also presented in Figure 4b, which is usually difficult to obtain directly in the experimental way. According to the diffraction data (see, e.g., ref 14), three peaks would be expected at 2.6, 2.9, and 3.2 Å, with the peak-area ratio 1:2:1, respectively (averaged structure model). In this respect, the nearest interaction (a) is the O−O bond surrounded by 16d metals, the second one (b) is between the 16d metal and 16c vacancy, and the distant one (c) placed between vacancies (Figure 6). However, the pcf of O−O in LiMn$_2$O$_4$ showed four broad peaks in Figure 4. The split peak should be observed in the second interaction, indicating deviation from averaged structure. Furthermore, dramatic change was observed with increasing Co content in the lattice: (i) the split peak around 2.9 Å disappeared and finally three peaks expected by the diffraction data were observed at the composition $y = 1$, and (ii) the shape of each peak became sharper.
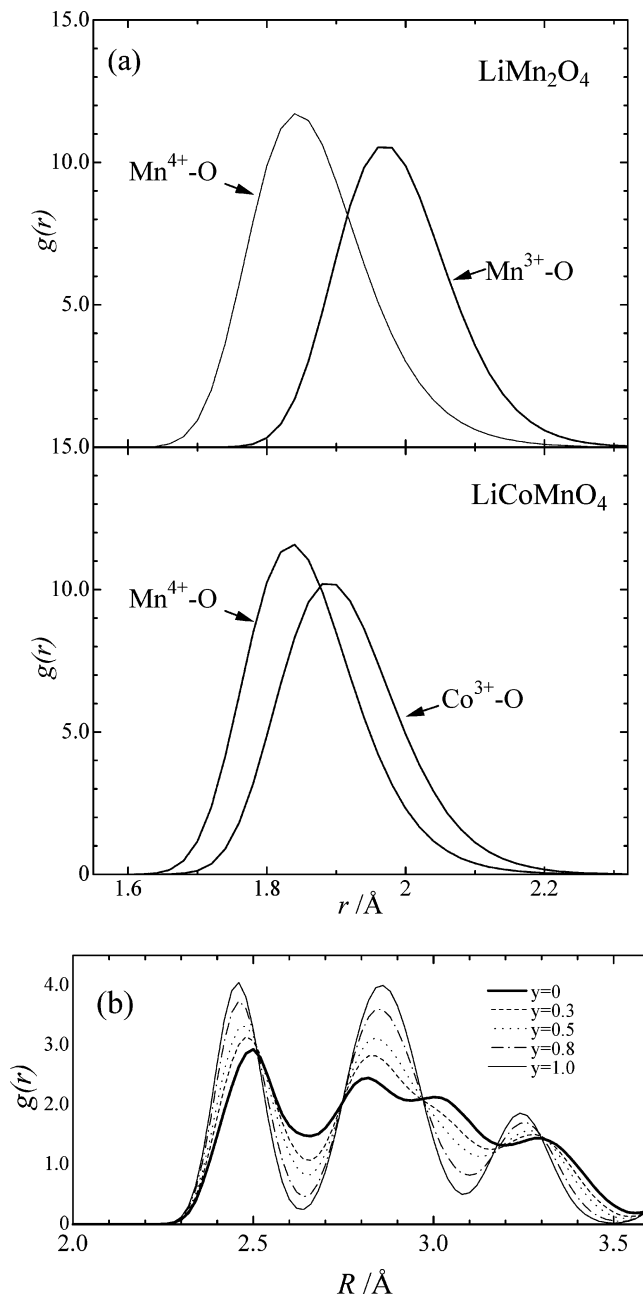

Figure 4. pcf of LiCo$_y$Mn$_{2-y}$O$_4$: (a) metal−oxygen interaction and (b) oxygen−oxygen interaction.

Hence, the former feature indicates that the Co substitution gives the lattice averaged structure, and the latter one corresponds to the decrease of the local distortion. Summing up the calculated pcf, the local structure, especially on the bond length, mainly depends on the ionic size of each cation, and the difference in cation size causes the lattice deviation from the average structure. In addition, the local distortion arising from a difference in the cation size seems to change the arrangement of the oxide ion, and presumably, the 16c site vacancy contributes to the distribution of oxide ions according to the data of O−O interaction (Figure 4b).

Finally, we investigated the dynamical properties of the lattice to evaluate the strength of the chemical bonds. Figure 7 shows the simulated vibrational DOS of each ion in LiMMnO$_4$ (M = Mn, Co, Cr). The relatively larger DOS was observed in the lower wavenumber region and corresponded to the acoustic branch of vibration, or translational mode of ionic motion. On the other hand, the DOS in the higher wavenumber region
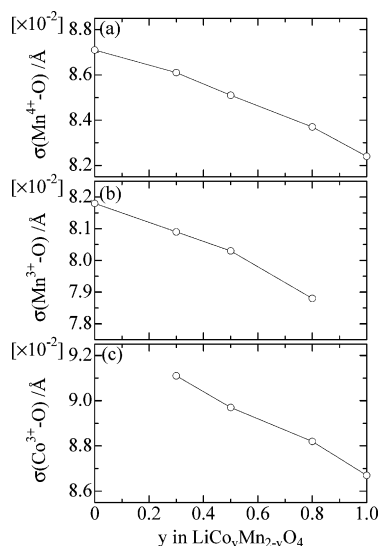
Figure 5. Variation of standard deviation in the first neighbor pcf peaks of M−O bonds as a function of y in LiCo$_y$Mn$_{2-y}$O$_4$.
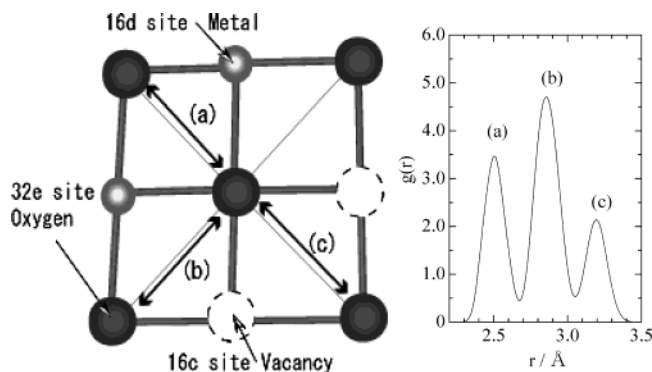

Figure 6. Expected pcf relationship between oxide ions based on the averaged structure. The left panel shows the atomic configuration in the spinel structure, and the right panel shows the expected pcf curve based on the ref 12 (the pcf peaks were broadened by adopting an appropriate distribution function).

represents the optical branch of vibration, directly related to the nature of the bond strength. In this region, the DOS of theoxide ion shows the dominant feature in the spectra, indicating that distribution of site potentials in the anion sites is broader than that in the cation sites. Figure 7d shows the magnification of the DOS for oxide ions in the higher wave-number region (>600 cm^{-1}). Compared with those for the nonsubstituted sample (LiMn$_2$O$_4$), the peaks of vibrational DOS shown in the Co and Cr substituted one clearly became sharper and shift to the higher wavenumber side in that order. The former behavior would correspond to the narrowed distribution of the site potentials of the oxide ion and would relate to the suppression of local distortion as mentioned in Figures 4 and 5. The latter one is directly related to the nature of the bond strength, and it is confirmed that the Co and/or Cr substituted spinels have stronger bonds than the nonsubstituted one. With respect to the relationship between calculated DOS (Figure 7) and experimental infrared absorption spectra (Figure 3), qualitative accordance was observed. The peak observed in 720 cm^{-1} for LiMn$_2$O$_4$ in Figure 7 would correspond to the T$_{1u}$ peak (620 cm^{-1}) in Figure 3. Despite the difference between calculated and experimental resonance wavenumbers ($\sim$100 cm^{-1}), both spectra show a similar peak shift on Co and/or Cr substitution, respectively. In detail, the Co doped sample, LiCoMnO$_4$, showed the peak at higher wavenumber 40−50 cm^{-1} than the peak
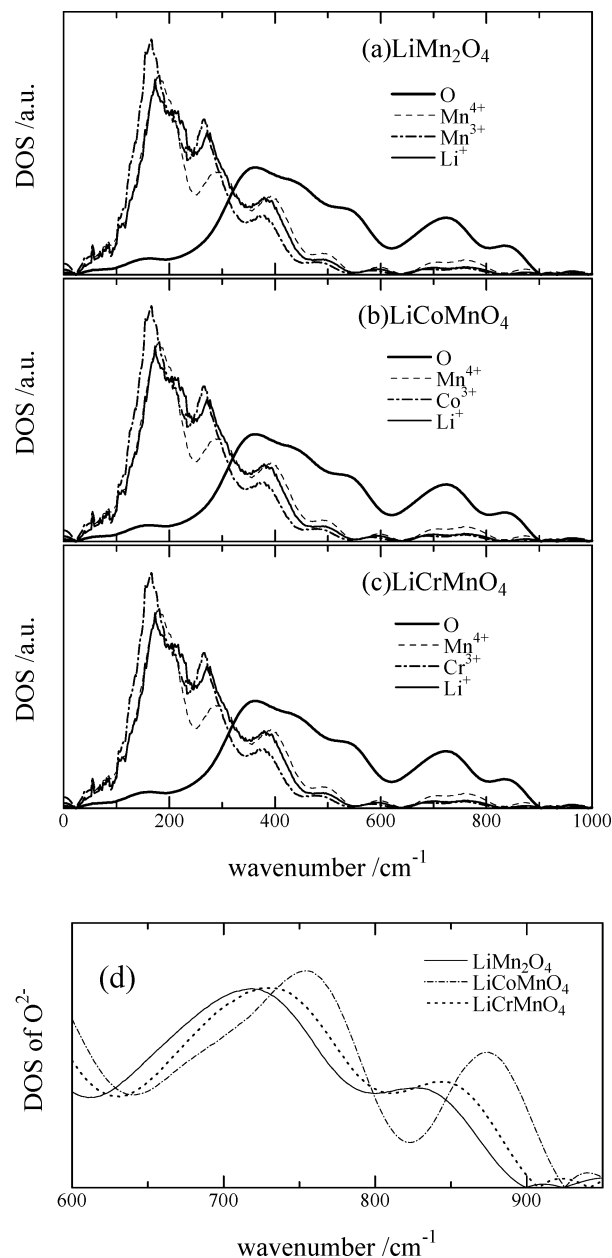

Figure 7. Vibrational DOS of each atom in (a) LiMn$_2$O$_4$, (b) LiCoMnO$_4$, and (c) LiCrMnO$_4$. (d) Vibrational DOS of the oxide ion at the higher wavenumber region (>600 cm^{-1}).

observed in LiMn$_2$O$_4$, and the peak of LiCrMnO$_4$ was observed at 20 cm^{-1} higher wavenumber than that of LiMn$_2$O$_4$ in both calculated and experimental vibrational spectra. Probably, the difference in absolute value of the resonance wavenumber is due to the potential parameters for MD simulation. As mentioned in our previous paper, the potential parameters were determined to reproduce the lattice parameters with various compositions and temperature. These changes in lattice parameters almost do not reflect the harmonic vibrations of the lattice; hence the calculated DOS of the higher wavenumber region deviate from the observed spectra. However, it was confirmed qualitatively that the bond strength was increased by the Co and/or Cr substitution based on both the experimental and calculated results. Note that the bond strength does not depend on the depth of site potential theoretically but associates with the sharpness of the site potential well[40] (the sharper the potential well, the stronger the bond). Accordingly, it would be concluded that the suppression of local distortion around the oxide ion

causes a sharper distribution of site potential around the oxide ion and leads to the reinforcement of chemical bonds.

Conclusion

Molecular dynamics simulation was carried out for Co doped lithium manganese oxide (LiCo$_y$Mn$_{2-y}$O$_4$). Obtained potential parameters for MD simulation are reproducible for the lattice parameters at room temperature and for thermal expansion coefficients. From the MD simulation for LiMn^{3+}Mn^{4+}O$_4$ and LiCo^{3+}Mn^{4+}O$_4$, the calculated results show that the distortion of MO$_6$ octahedra decreases with cobalt doping, and the analysis of simulated results showed the importance of the size difference of cations. Furthermore, the positive relationship between local structure and bond strength was observed through the analysis of dynamic properties of MD simulation, indicating the shape of the potential well strongly depends on the local structure around the oxide ion. Although there is not yet clear theoretical evidence of the relationship between the nature of the bond strength and the cyclability of Li ion batteries, the reinforcement of the chemical bond observed in the Co(Cr) doped spinel seems to be one of the possible reasons for the improvement of cyclability.

References and Notes

(1) Scrosati, B. *Nature* **1995**, *573*, 557. Scrosati, B. *Electrochim. Acta* **2000**, *45*, 2461.

(2) Wakihara, M.; Li, G.; Ikuta, H. *Lithium Ion Batteries*; Koudansha: New York, 1998; Chapter 2.

(3) Guyomard, D. *Energy Storage Systems for Electronics*; Gordon and Breach Science Publishers: Singapore, 2000; Chapter 9.

(4) Bittihn, R.; Herr, R.; Hoge, D. *J. Power Sources* **1993**, *43−44*, 223.

(5) Li, G.; Ikuta, H.; Uchida, T.; Wakihara, M. *J. Electrochem. Soc.* **1996**, *143*, 178.

(6) Gummow, R. J.; Kock, A. de; Thackeray, M. M. *Solid State Ionics* **1994**, *69*, 59.

(7) Robertson, A. D.; Lu, S. H.; Averill, W. F.; Howard, W. F., Jr. *J. Electrochem. Soc.* **1997**, *144*, 3500.

(8) Robertson, A. D.; Lu, S. H.; Howard, W. F., Jr. *J. Electrochem, Soc.* **1997**, *144*, 3505.

(9) Cras, F. Le; Bloch, D.; Anne, M.; Strobel, P. *Solid State Ionics* **1996**, *89*, 203.

(10) Pistoia, G.; Wang, G. *Solid State Ionics* **1993**, *66*, 135.

(11) Tarascon, J. M.; Wang, E.; Shokoohi, F. K.; McKinnon, W. R.; Colson, S. *J. Electrochem. Soc.* **1991**, *138*, 2589. Xia, Y.; Zhou, Y.; Yoshio, M. *J. Electrochem. Soc.* **1997**, *144*, 2593.; Jang, D. H.; Oh, S. M. *J. Electrochem. Soc.* **1997**, *144*, 3342.; Song, D.; Ikuta, H.; Wakihara, M. *Electrochemistry* **2000**, *68*, 460.

(12) Yamada, A.; Tanaka, M. *Mater. Res. Bull.* **1995**, *30*, 715. Yamada, A. *J. Solid State Chem.* **1995**, *122*, 160.

(13) Ohzuku, T.; Kitagawa, M.; Hirai, T. *J. Electrochem. Soc.* **1990**, *137*, 769.

(14) Oikawa, K.; Kamiyama, T.; Izumi, F.; Nakazato, D.; Ikuta, H.; Wakihara, M. *J. Solid State Chem.* **1999**, *146*, 322.

(15) Berg, H.; Thomas, J. O. *Solid State Ionics* **1999**, *126*, 227.

(16) Rodríguez-Carvajal, J.; Rousse, G.; Masquelier, C.; Hervieu, M. *Phys. Rev. Lett.* **1998**, *81*, 4660.

(17) Oikawa, K.; Kamiyama, T.; Izumi, F.; Chakoumakos, B. C.; Ikuta, H.; Wakihara, M.; Li, J.; Matui, Y. *Solid State Ionics* **1998**, *109*, 35.

(18) Ammundsen, B.; Jones, D. J.; Rozière, J. *Chem. Mater.* **1996**, *8*, 2799.

(19) Shiraishi, Y.; Nakai, I.; Tsubata, T.; Himeda, T.; Nishikawa, F. *J. Solid State Chem.* **1997**, *133*, 587.

(20) Ammundsen, B.; Jones, D. J.; Rozière, J. *J. Phys. Chem. B* **1998**, *102*, 7939.

(21) Aitchison, P.; Ammundsen, B.; Jones, D. J.; Burns G.; Roziere, J. *J. Mater. Chem.* **1999**, *9*, 3125.

(22) Treuil, N.; Labrugère, C.; Menetrier, M.; Portier, J.; Campet, G.; Deshayes, A.; Frison, J.-C.; Hwang, S.-J.; Song, S.-W.; Choy, J.-H. *J. Phys. Chem. B* **1999**, *103*, 2100.

(23) Nakai, I.; Yasaka, K.; Sasaki, H.; Terada, Y.; Ikuta, H.; Wakihara, M. *J. Power Sources* **2001**, *97*, 412.

(24) Kaneko, M.; Matsuno, S.; Miki, T.; Nakayama, M.; Ikuta, H.; Uchimoto, Y.; Wakihara, M.; Kawamura, K. *J. Phys. Chem. B* **2003**, *107*, 1727.

(25) Ammundsen, B.; Rozière, J.; Islam, M. S. *J. Phys. Chem. B* **1997**, *101*, 8156.

(26) Ammundsen, B.; Burns, G. R.; Islam, M. S.; Kanoh, H.; Rozière, J. *J. Phys. Chem. B* **1999**, *103*, 5175.

(27) Ammundsen, B.; Islam, M. S.; Jones, D. J.; Rozière, J. *J. Power Sources* **1999**, *81−88*, 500.

(28) Islam, M. S.; Ammundsen, B. Computer Modelling of Oxide Cathode Materials for Lithium Ion Batteries. In *Materials for Lithium Ion Batteries*; Julien, C., Stoynov, Z., Eds.; NATO-ASI Series; Kluwer Academic: Dordrecht, The Netherlands, 2000; p 279.

(29) Braithwaite, J. S.; Catlow, C. R. A.; Harding, J. H.; Gale, J. D. *Phys. Chem. Chem. Phys.* **2000**, *2*, 3841.

(30) Suzuki, K.; Oumi, Y.; Takami, S.; Kubo, M.; Miyamoto, A.; Kikuchi, M.; Yamazaki, N.; Mita, M. *Jpn. J. Appl. Phys.* **2000**, *39*, 4318.

(31) Tateishi, K.; Boulay, D. D.; Ishizawa, N.; Kawamura, K. *J. Solid State Chem.* **2003**, *174*, 175.

(32) Islam, M. S.; Catlow, C. R. A. *J. Solid State Chem.* **1988**, *77*, 180. Islam, M. S. *Philos. Mag. A* **1993**, *68*, 667.

(33) Julien, C. M.; Massot, M. *J. Power Sources* **2003**, *119−121*, 743. Julien, C. M.; Massot, M. *Mater. Sci. Eng. B* **2003**, *97*, 217. Julien, C. M.; Massot, *M. Mater. Sci. Eng. B* **2003**, *100*, 69.

(34) Katsumata, T.; Inaguma, Y.; Itoh, M.; Kawamura, K. *Chem. Mater.* **2002**, *14*, 3930.

(35) Kawamura, K. MXDORTO, Japan Chemistry Program Exchange, #029.

(36) Marin, S. J.; O'Keeffe, M.; Partin, D. E. *J. Solid State Chem.* **1994**, *113*, 413. Idemoto, Y.; Narai, H.; Koura, N. *J. Power Sources* **2003**, *119−121*, 125.

(37) Hayashi, N.; Ikuta, H.; Wakihara, M. *J. Electrochem. Soc.* **1999**, *146*, 1351.

(38) Strobel, P.; Palos, A. I.; Anne, M.; Cras, F. L. *J. Mater. Chem.* **2000**, *10*, 429.

(39) Strobel, P.; Palos, A. I.; Anne, M.; Poinsignon, C.; Crisci, A. *Solid State Sci.* **2003**, *5*, 1009.

(40) For example, Nakamoto, K. *Infrared and Raman Spectra of Inorganic and Coordination Compounds*; John Wiley & Sons: New York, 1986.

(41) Shannon, R. D. *Acta Crystallogr.* **1976**, *A32*, 751.